Available online at www.sciencedirect.com
ScienceDirect
Journal of Nuclear Materials 363–365 (2007) 1246–1250
journal of nuclear materials
www.elsevier.com/locate/jnucmat

# Tungsten coatings for the JET ITER-like wall project

H. Maier [a,*], R. Neu [a], H. Greuner [a], Ch. Hopf [a], G.F. Matthews [b], G. Piazza [c], T. Hirai [d], G. Counsell [b], X. Courtois [e], R. Mitteau [e], E. Gauthier [e], J. Likonen [f], G. Maddaluno [g], V. Philipps [d], B. Riccardi [g], C. Ruset [h], EFDA-JET Team [1]

[a] *Max-Planck-Institut für Plasmaphysik, EURATOM Association, D-85748 Garching, Germany*
[b] *Association EURATOM–UKAEA, Culham Science Centre, Abingdon, UK*
[c] *EFDA-Close Support Unit, Culham Science Centre, Abingdon, UK*
[d] *Association EURATOM–Forschungszentrum Jülich (FZJ), D-52425 Jülich, Germany*
[e] *Association EURATOM–CEA, Cadarache, DSM/DRFC, 13108 Saint Paul Lez Durance, France*
[f] *Association EURATOM–TEKES, VTT, P.O. Box 1000, 02044 VTT, Finland*
[g] *Association EURATOM–ENEA, Frascati, Italy*
[h] *National Institute for Laser, Plasma and Radiation Physics, Association EURATOM–MEdC, Bucharest, Romania*

**Abstract**

In the frame of JET's ITER-like wall project for most of the divertor surface tungsten coatings are intended to be employed on bidirectionally carbon fibre reinforced carbon substrates. Since this is thermomechanically rather mismatched, a variety of deposition conditions were considered. Mostly in cooperation with industry, five Euratom associations provided 14 different types of samples with respect to production method and coating thickness. In a step-wise selection procedure, these were subjected to a thermal screening test and a thermal cycling test in the ion beam facility GLADIS as well as to an ELM-like thermal shock test in the electron beam facility JUDITH. A general failure mode is crack formation upon cool-down. Coatings with several microns of thickness show a distinct delamination feature in addition. Further analysis included metallographic investigation, X-ray diffraction for film stress assessment, adhesion testing as well as measurements on the contents of light impurities.


*PACS:* 52.55.Fa; 62.20.Mk; 65.70.+y; 81.15.−z

*Keywords:* Coating; Divertor material; Electron beam; JET; Tungsten

## 1. Introduction

The operational behaviour and the interplay of the ITER plasma facing materials choice has never been investigated in a tokamak experiment. This motivated the ITER-like wall project at JET, in which the main chamber will be equipped with Be

* Corresponding author. Fax: +49 893299 7272.
*E-mail address:* Hans.Maier@ipp.mpg.de (H. Maier).
[1] See annex of J. Pamela et al., "Overview of JET Results" (Proc. 20th IAEA Fusion Energy Conference, Vilamoura, Portugal, 2004).

0022-3115/$ - see front matter © 2007 Elsevier B.V. All rights reserved.
doi:10.1016/j.jnucmat.2007.01.246

as plasma-facing material, and in parallel a completely tungsten-clad divertor will be installed, mainly consisting of tungsten coatings [1,2]. Scientific goals of this project include general questions of plasma operation with a low melting Be wall, compatibility of all envisaged ITER scenarios with a W divertor, tritium retention and removal and mixed materials effects, erosion behaviour and lifetime investigations.

After an R&D phase involving 5 EURATOM associations, the output of this R&D was investigated to qualify a method for coating CFC with tungsten. The main body of results was achieved by high heat flux testing in the GLADIS facility at IPP Garching, Germany [3]. Besides a high heat flux screening procedure to determine the ultimate loading conditions for each type of coating, the thermomechanical mismatch of tungsten and CFC called for an explicit investigation of the fatigue behaviour of these coatings. High cycle fatigue experiments at moderate loading conditions were out of reach due to the time constraints of the ITER-like wall project. Therefore a program for low-cycle fatigue experiments (200–300 cycles) was proposed and adopted. ELM-like loading was performed in the JUDITH facility at FZ Jülich, Germany up to 1000 cycles [4].

In addition, adhesion tests, metallographic examination, X-ray diffraction for stress analysis, and the measurement of the impurity contents were conducted as well as an R&D program on non-destructive testing.

## 2. Sample types

The ASDEX Upgrade tungsten program has proven that the rather inexpensive solution of tungsten coatings is feasible on fine grain graphite [5,6]. For CFC, however, a new test program was necessary because of the micro- and macroscopic thermal expansion mismatch with tungsten.

Samples from a variety of coating processes and manufacturers were investigated for risk minimisation. In addition, it was agreed that three different coating thicknesses were to be investigated. These can be separated into two groups called ‘thick’ and ‘thin’ coatings here. The thick coatings had a target value of 200 μm and the thin coatings had two different target values of 4 μm and 10 μm, respectively. Four microns is a value, which has already been employed in the past to coat CFC substrates for smaller-sized test coatings for exposure in the JET divertor [7,8]. In the mean time it has, however, been found that 4 μm is an insufficient thickness for distinct areas of the outer divertor from an erosion lifetime point of view [8].

Coating research and development was performed by CEA France, ENEA Italy, IPP Garching Germany, MEdC Romania, TEKES Finland, mostly in cooperation with industry. The deposition methods employed were chemical vapour deposition (CVD), different types of physical vapour deposition (PVD), as well as vacuum plasma spraying (VPS). The total number of different coating thickness/deposition method combinations resulted in 14. The majority of the samples were machined with the fibre planes perpendicular to the surface corresponding to the orientation for all divertor tiles.

## 3. High heat flux tests

### 3.1. Experimental

High heat flux testing was performed in three consecutive steps the two first steps being conducted in the GLADIS facility at IPP Garching: First, all samples were subjected to a thermal screening procedure with increasing power density and pulse duration steps given in Table 1 together with typical peak surface temperatures. Fresh samples were subjected to cyclic loading to investigate their fatigue behaviour. This was performed at 10.5 $MW/m^2$ for 5 s with 200–300 repetitions.

For the high heat flux loading in the GLADIS facility the samples were mounted in sets of two onto a water-cooled holder with a flexible carbon sheet for good thermal contact. While in the screening the ion beam was centered onto the individual tile, the cyclic loading was performed onto pairs of tiles in order to save time. The contact pressure was kept approximately constant during temperature cycles by employing two disk spring stacks per tile. The period between pulses was set such that the tile temperature measured by thermocouples always was below 200 °C before pulse start. This waiting time was typically 3 min. The standard diagnostics used in GLADIS were one- and two-colour pyrometry, an infrared camera taking frames for 10 s during each pulse at a rate of 10 Hz and a CCD video camera.

Finally, a further reduced number of cycled samples was exposed to ELM-like loading at FZ Jülich. Here surface areas of $8 \times 8$ $mm^2$ were subjected to 1,

Table 1
Nominal central power densities of employed beam profiles, pulse durations, and corresponding typical peak surface temperatures at pulse end

| Power density | P1 | P2 | P3 | P4 | P5 |
|---|---|---|---|---|---|
| Centr. value | 6.0 MW/m$^2$ | 7.5 MW/m$^2$ | 10.5 MW/m$^2$ | 16.5 MW/m$^2$ | 23.5 MW/m$^2$ |
| Durations [s] | 6.0, 7.5, 10.0 | 5.0, 7.5 | 2.0, 4.0, 5.0, 6.0 | 2.0, 3.0 | 1.0, 1.5 |
| Peak surf. temp. | 1300 (10.0 s) | 1500 (7.5 s) | 1700 (6.0 s) | 1850 (3.0 s) | 2200 (1.5 s) |

10, 100, and 1000 pulses of 1 ms duration at a typical ELM power density of 0.35 GW/m$^2$. The energy deposited per pulse was 23 J. Due to a defective pyrometer, the temperature rise could not be measured, but is estimated to be about 640 °C at pulse end (based on bulk-W data). The pulses were applied with a repetition frequency of 0.3 Hz. The bulk temperature increase was 40 K after 1000 pulses.

### 3.2. Results and discussion

The coatings discussed here were applied onto the $x$–$y$ surface with fibres running in the $y$-direction and perpendicular to the surface in $z$-direction and no fibres in $x$-direction, see Fig. 1. Therefore the thermal expansion of the substrate is larger than that of the coating in the $x$-direction and smaller in the $y$-direction.

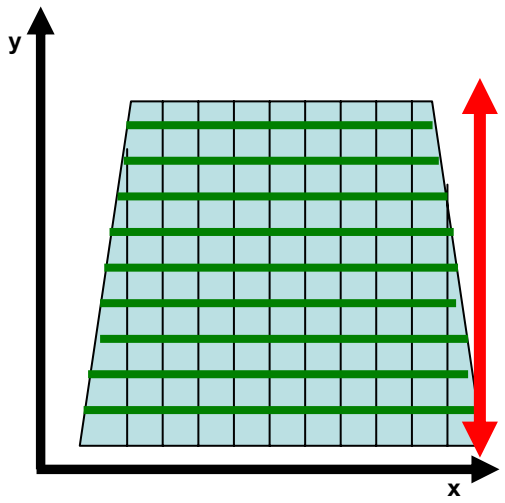


Fig. 1. Schematic representation of the employed coordinates and the fibre orientation. The thin vertical lines in $y$-direction represent the fibre orientation on the tile surface. The righthand vertical arrow indicates the direction of tensile coating stress upon cool-down. The thick horizontal lines in $x$-direction represent the resulting tensile cracks, i.e. failure mode 1. The size is $80 \times 80$ mm$^2$.

All observed failure features of the tungsten coatings were oriented such that it can be concluded that they occurred upon cool-down of the samples after the pulses. As soon as the surface temperature reaches values, where stress relaxation can occur with sufficient efficiency, i.e. fast enough, the stress state of the films will tend to change towards $\sigma = 0$. Mechanisms for this are plastic deformation in general, creep, or recrystallisation. It is important to mention here, that all of the above mechanisms are thermally activated processes. This means that the rate, at which they occur depends exponentially on temperature. Therefore the stress relaxation may occur in a single pulse at sufficiently high temperature or it may occur incrementally with increasing pulse number at lower peak temperatures.

A general failure mode (mode 1) common to all samples irrespective of the coating thickness or deposition method was the formation of tensile cracks running parallel to the $x$-direction as shown in Fig. 1. As mentioned above, the given orientation indicates that this crack formation is due to tensile load of the coatings during cool-down. For this, high-temperature stress relaxation must have occurred. As indicated in Fig. 1, these cracks formed laterally repetitive with a typical distance for a given coating thickness. For the 200 μm coatings for instance, a simple force balance estimate yields a typical distance of 4 mm assuming the mechanical properties of bulk tungsten [9], which is in fact mostly in agreement with observation.

In the thermal screening, besides failure mode 1, one 200 μm VPS and one 200 μm CVD coating failed by delamination and subsequent melting at power densities P1 and P5, respectively. Three of the thin coatings displayed localised delamination and melting. Since this occurred on a sub-mm scale, it could only be investigated by microscopy after completion of the program.

The cyclic loading program additionally revealed two distinct general failure modes for the thin coatings, both attributed to fatigue upon repeated heating/cooling cycles. These are clearly visible in Fig. 2.


Fig. 2. Secondary electron SEM image of a 4 µm PVD coating after cyclic loading in the GLADIS facility. The horizontal cracks correspond to the tensile failure mode 1, as explained in the text. The buckling of debonded areas (failure mode 2) as well as the subsequent formation of fatigue cracks in the *y*-direction (failure mode 3) can also be clearly distinguished.

They are buckling of unbonded areas and crack formation in *y*-direction. As a stress-relaxed coating is subjected to compression in *x*-direction upon cool-down, debonded areas form, which buckle upwards as a reaction to this compressive stress (mode 2). The repeated flattening and re-forming of these buckles upon repeated heating/cooling cycles leads to the formation of fatigue cracks (mode 3) running in *y*-direction. Only the CMSII coating with a Mo interlayer, which had reduced intrinsic stress compared to that expected without ion implantation, did not show these fatigue phenomena.

For the thick coatings the cyclic loading program did not reveal any specific common fatigue phenomena. In some cases, however, mm- to cm-sized delaminations occurred. These areas are clearly observable at an early failure stage in the IR camera data during a pulse, because they overheat with respect to the surrounding surface. Melting occurs when the heat removal path becomes insufficient as compared to the power input. The lefthand side of Fig. 3 shows an IR camera frame of such a failure which is developing during the cyclic loading program. The frame is taken early during the pulse at 2.0 s. To further illustrate the hot spots on the tile, the righthand side of the figure shows a linescan taken from the IR frame and calibrated to temperature assuming an emissivity of 0.25. The linescan is taken along the whole tile from top to bottom through the hot spots. For this sample, melting occurred 20 pulses after the first visible anomaly.

Finally, after the ELM-like loading step to 1000 pulses, it was concluded that all three discussed failure modes were observed on all thin coatings. The thick coatings, in contrast, were thermomechanically unaffected by this loading step. This is interpreted to be due to the thickness of the coatings: The thermal expansion mismatch is alleviated by the fact that the pulse duration is shorter than the travel time of the heat wave through the coating to the interface. In addition, electron microscopy did not show any localised melting for thick coatings.

## 4. Further investigations

Impurity analysis was performed at FZ Jülich by secondary ion mass spectrometry in combination with sputter depth profiling. In parallel, carbon and oxygen impurities were investigated at IPP Garching by nuclear reaction analysis using a deuterium ion beam. The results from these analyses did not clearly exceed the specified impurity limits (10 at.% for C and 5 at.% for O) or reveal distinct differences between the analysed sample types.

The adhesion of the coatings was investigated by performing a tensile test on steel cylinders glued onto the coatings surfaces. Again these results were inconspicuous except for one VPS coating type, which barely exceeded the specified threshold.

For the thin coatings, an X-ray stress analysis was performed direction dependent, since the substrates are anisotropic. The results clearly divide into two groups: While all CVD coatings show a moderate stress level with a direction dependent change of sign from typically −100 MPa to +200 MPa, all PVD coatings show considerable compressive stress in all directions along the sample surface. Compressive stress is generally expected for energetic PVD processes [10] and is experimentally

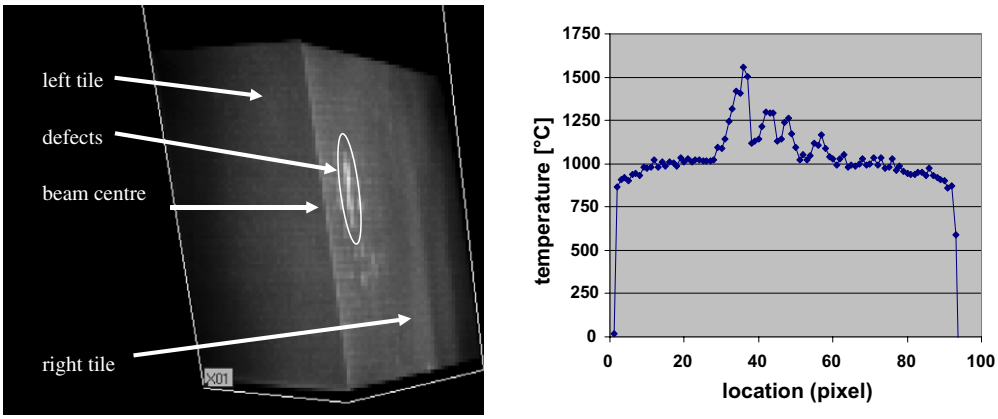


Fig. 3. Lefthand: Infrared camera frame showing hot spots on a 200 μm VPS sample during cyclic loading at $t = 2.0$ s, which indicates the beginning of delamination. Righthand: Vertical linescan through the hot spots. Data taken from a vertical pixel column and calibrated assuming an emissivity of 0.25.

observed especially for magnetron sputtering of metals [11].

Finally, the metallographic examination of polished cross-sections revealed, that for a highly porous material like CFC CVD is far superior to PVD methods with respect to good surface coverage, since the CVD coating grows on all surfaces, also inside pores.

## 5. Conclusions and consequences

From the results presented in this contribution it must be concluded that micrometer CVD or PVD coatings on CFC cannot be employed for high power loaded areas in the JET divertor. Therefore a 200 μm solution will have to be employed. On these coatings, however, some obtained results were not sufficiently conclusive. An R&D program on non-destructive testing by IR thermography proved this method to be incapable of predicting the delamination failures observed during the high heat load test campaign. As a consequence, reliable quality assurance can only be obtained by combining moderate heat flux cycling with IR thermography.

## References

[1] J. Paméla et al., J. Nucl. Mater., these Proceedings, doi: 10.1016/j.jnucmat.2006.12.056.
[2] G. Piazza et al., J. Nucl. Mater. Special issue ICFRM-12.
[3] H. Greuner et al., Fus. Eng. Des. 75 (9) (2005) 333.
[4] R. Duwe, W. Kühnlein, M. Münstermann, in: Proc. SOFT 1994, Fus. Technol. (1995) 335.
[5] R. Neu et al., J. Nucl. Mater., these Proceedings, doi: 10.1016/j.jnucmat.2006.12.021.
[6] H. Maier, Mat. Sci. Forum 475–479 (2005) 1377, and references therein.
[7] S. Lehto, J. Likonen, J.P. Coad, T. Ahlgren, D.E. Hole, M. Mayer, H. Maier, P. Andrew, J. Kolehmainen, Fusion Eng. Des. 66–68 (2003) 241.
[8] M. Mayer et al., J. Nucl. Mater., these Proceedings, doi: 10.1016/j.jnucmat.2007.01.010.
[9] Courtesy J.H. You, Max-Planck-Institut für Plasmaphysik, Garching, Germany.
[10] G. Carter, J. Phys. D – Appl. Phys. 27 (5) (1994) 1046.
[11] J.A. Thornton, D.W. Hoffman, Thin Solid Films 171 (1989) 5, and references therein.